Applied Physics Letters

High power factor in epitaxial Mg_2Sn thin films via Ga doping

Cite as: Appl. Phys. Lett. **119**, 254101 (2021); https://doi.org/10.1063/5.0074707
Submitted: 11 October 2021 • Accepted: 29 November 2021 • Published Online: 20 December 2021

Mariana S. L. Lima, Takashi Aizawa, Isao Ohkubo, et al.

COLLECTIONS

Paper published as part of the special topic on Thermoelectric Materials Science and Technology Towards Applications

ARTICLES YOU MAY BE INTERESTED IN

Valence band convergence and nanostructured phonon scattering trigger high thermoelectric performance in SnTe
Applied Physics Letters **119**, 253901 (2021); https://doi.org/10.1063/5.0076989

MEMS post-processed self-assembled electret for vibratory energy harvesters
Applied Physics Letters **119**, 254102 (2021); https://doi.org/10.1063/5.0072596

Equilibrium charge state of NV centers in diamond
Applied Physics Letters **119**, 254001 (2021); https://doi.org/10.1063/5.0079687

© 2021 Author(s).

High power factor in epitaxial Mg_2Sn thin films via Ga doping

Cite as: Appl. Phys. Lett. **119**, 254101 (2021); doi: 10.1063/5.0074707
Submitted: 11 October 2021 · Accepted: 29 November 2021 ·
Published Online: 20 December 2021

Mariana S. L. Lima,[1,2] Takashi Aizawa,[2] Isao Ohkubo,[2] Takahiro Baba,[1,2] Takeaki Sakurai,[1,a)] and Takao Mori[1,2,a)]

AFFILIATIONS

[1]Graduate School of Pure and Applied Sciences, University of Tsukuba, 1-1-1-Tennodai, Tsukuba, Ibaraki 305-8573, Japan
[2]International Center for Materials Nanoarchitectonics (WPI-MANA), National Institute for Materials Science (NIMS), 1-1 Namiki, Tsukuba, Ibaraki 305-0044, Japan

Note: This paper is part of the APL Special Collection on Thermoelectric Materials Science and Technology Towards Applications.
[a)]**Authors to whom correspondence should be addressed:** sakurai@bk.tsukuba.ac.jp and MORI.Takao@nims.go.jp

ABSTRACT

In this work, we present the influence of Ga doping in Mg_2Sn thin epitaxial films on sapphire (0001) substrates. Our results suggest that epitaxial nature is essential for achieving high mobility. Furthermore, we found that Ga incorporation influences the carrier concentration and acts as a phonon-scattering center. The optimal power factor and figure of merit values obtained were 1.49×10^{-3} W·m^{-1}·K^{-1} and 0.08 at 300 K for $Mg_2Sn_{0.97}Ga_{0.03}$. The values are in the same range as the bulk material of Mg-based II–IV semiconductors, suggesting that the combination of doping and epitaxial nature in thin films can be a promising route for miniaturization of thermoelectric devices based on Mg-based materials.

© 2021 Author(s). All article content, except where otherwise noted, is licensed under a Creative Commons Attribution (CC BY) license (http://creativecommons.org/licenses/by/4.0/). https://doi.org/10.1063/5.0074707

Thermoelectricity is a promising alternative for power generation because of its ability to convert waste heat into electricity via the Seebeck effect.[1–4] The efficiency of the thermoelectric generators (TEGs) is determined by the balance between electrical and thermal properties. This balance is evaluated by the dimensionless figure of merit, $ZT = \alpha^2\sigma T/\kappa$, where α, σ, T, and κ are the Seebeck coefficient, electrical conductivity, absolute temperature, and thermal conductivity, respectively. An efficient thermoelectric material should have a high power factor ($PF = \alpha^2\sigma$) and low κ. There are conventional trade-off relations between the individual thermoelectric properties, and effective strategies are needed for enhancement.[5–8] For higher device performance, both n-type and p-type legs and high ZT are required.

In the past years, Mg-based II–IV semiconductors with a narrow bandgap (~0.7 eV in the case of Mg_2Si and Mg_2Ge and ~0.3 eV for Mg_2Sn) and their solid solutions ($Mg_2Sn_{1-x}Si_x$, $Mg_2Sn_{1-x}Ge_x$, and $Mg_2Si_{1-x}Ge_x$) have been studied as promising low-cost alternatives for thermoelectric applications.[9,10] An effective approach to improve the thermoelectric properties of Mg-based II–IV semiconductors is the combination of single crystals and doping.[11–16] In polycrystals, there exist many grain boundaries of large crystallographic angle difference, which can act not only as scatterers of carriers but also as trapping sites. Additionally, they can make interface energy levels that can cause band bending through the pinning effect. On the contrary, single crystals have a large grain size and free from such disturbances, to improve the mobility and, consequently, the conductivity.

Doping influences all the parameters of the ZT. In the PF, doping acts to optimize the carrier concentration by improving the conductivity and shifting the maximum peak of the Seebeck coefficient from the bipolar effect.[17] In thermal conductivity, doping can act as a phonon-point defect scattering center, reducing the thermal lattice contribution. However, for all the effects to occur simultaneously, some criteria in the choice of doping must be considered, such as atomic mass, ionic radii, position in the periodic table, and formation energy. For instance, in the case of n-type, the Sb-doped-Mg_2Sn single crystal has achieved a ZT of approximately 1 at 650 K.[13] The high performance is a consequence of efficient Sb doping because of the negative formation energy in the Sn site,[18] and the difference in ionic radius between Sn and Sb is small, which facilitates the incorporation[19] and belongs to group 15 in periodic table that has one more valence electron. Therefore, the choice of doping is important toward improving the thermoelectric properties. In addition, it is essential to find good doping for the p-type material in this system, whose performance is still low.

For miniaturizing thermoelectric devices and their application to the Internet of Things (IoT), thin films are attracting attention and are

© Author(s) 2021

expected to be a promising component at room temperatures.[20,21] However, Mg-based II–IV semiconductor thin film fabrication is challenging owing to the difference in the melting point of Mg, Sn, Si, and Sn.[22,23] In addition, the high Mg vapor pressure requires fabrication in an Mg-rich regime to avoid the formation of secondary phases.[24,25] If we consider that the epitaxial film has a behavior similar to that of a single crystal, a promising approach is the combination of doping and epitaxy. However, reports on doping are limited to polycrystalline thin films.[26,27] Typically, the reported PF is one order lower than that of bulk materials.

We have recently reported $Mg_2Sn_{1-x}Ge_x$ epitaxial thin films by molecular beam epitaxy (MBE). The optimal PF value was 0.27×10^{-3} $W{\cdot}m^{-1}{\cdot}K^{-1}$ at 300 K.[25] In this Letter, we report the combination of doping and epitaxy to improve the thermoelectric properties of Mg_2Sn thin films. Herein, Ga was chosen as a dopant based on the following criteria: (i) in a Mg-rich regime, the formation energy is negative at the Sn site,[18] which facilitates the incorporation of doping into the thin film, (ii) its position in the periodic table suggests the appropriate doping type in relation to Sn. In our case, we wanted to form a p-type dopant. We chose the Sn site as the dopant because of the high vapor pressure of Mg, (iii) the difference in atomic mass between Sn and the dopant for the formation of a mass-point defect center, and (iv) the ionic radius must be close to Sn to maintain the epitaxy in our thin film. The combination of these criteria was responsible for the high PF in the thin film.

The $Mg_2Sn_{1-x}Ga_x$ ($0 < x < 0.1$) films were grown on sapphire (0001) substrates (Shinkosha, $\phi = 50.8 \pm 0.3$ and thicknesses of 0.43 ± 0.05 mm) using an MBE system (Eiko, EV-500) under vacuum conditions of 10^{-6}–10^{-7} Pa. The substrates were cleaned ultrasonically in acetone and subsequently heated at 1000 °C for 1 h in the MBE chamber before film growth. Elemental magnesium (99.95%, Furuuchi Chemical), tin (99.999%, Furuuchi Chemical), and gallium (99.999%, Nilaco) metals were evaporated using a conventional effusion cell at 380–480 °C for Mg, 1120–1180 °C for Sn, and 750–850 °C for Ga in a crucible of pyrolytic boron nitride (PBN). The relationship between the evaporation rate and cell temperature was determined using a retractable quartz crystal microbalance (QCM) thickness monitor (Q-pod, Inficon), located at the substrate position (Table S1 and Fig. S1, in the supplementary material). The nominal composition was calculated from the evaporation rate. The uncertainties were obtained from standard deviation of several measurements. Based on our previous study, we fixed the substrate temperature at 400 °C.[24] The film surface crystallinity can be observed *in situ* using reflection high-energy electron diffraction (RHEED), with a 15-keV electron beam, as shown in Fig. S2 in the supplementary material. The details of the experimental conditions and growth conditions process are described in the supplementary material.

Figure 1(a) shows the x-ray diffraction (XRD) pattern evolution with the Ga concentration in the Mg_2Sn thin films. All the samples exhibit just strong Mg_2Sn (*hkl*) peaks ($h = k = l = 1$–3), which can be indexed to a cubic antifluorite crystal structure with the group space *Fm-3m* (ICSD #151368). In addition, the peaks (0006) and (00012) from the Al_2O_3 substrate were observed, which can be indexed to a corundum trigonal with the group space *R-3c* (ICSD #93096). The XRD and RHEED (Fig. S2 in the supplementary material) patterns have similar behavior of our previous report, suggesting that the epitaxy relationship is $(111)_{Mg_2Sn} \| (0001)_{Al_2O_3}$ and $[11\bar{2}]_{Mg_2Sn} \| [10\bar{1}0]_{Al_2O_3}$.[24]

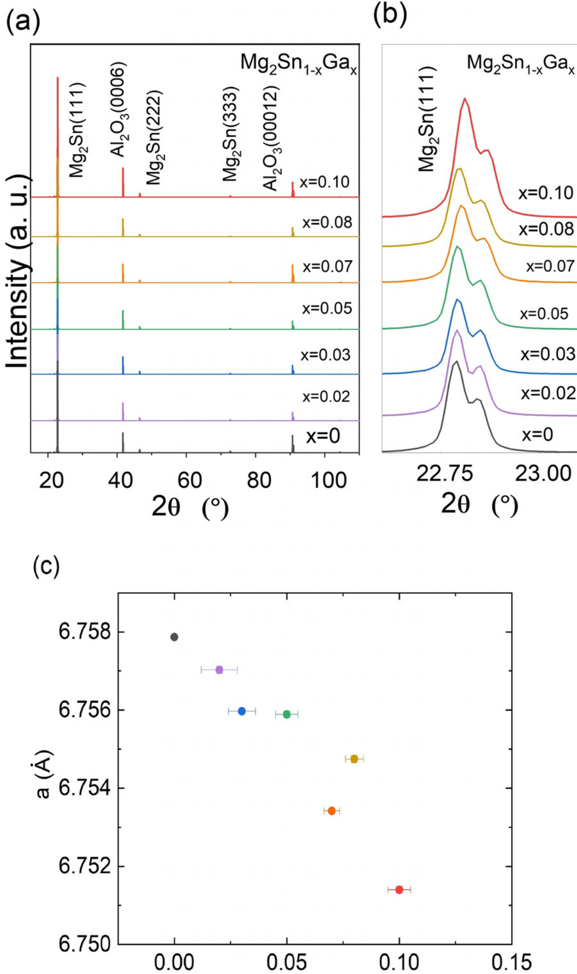

FIG. 1. (a) XRD patterns of the $Mg_2Sn_{1-x}Ga_x$ thin films recorded at room temperature. (b) The peaks shift on Mg_2Sn (111) and (c) the evolution of lattices parameters with Ga concentration.

Figure 1(b) shows the peak shift at $Mg_2Sn_{1-x}Ga_x$ (111), indicating a reduction in the lattice parameters, suggesting the substitution of Ga in the Sn site. In addition, no change in the shape was observed, suggesting a small difference in the d-spacing inside the material; consequently, the stress was small. These two facts are a consequence of the two criteria: the negative energy of formation of Ga in the Sn site and the crystal radius of Ga (61 pm) being smaller than that of Sn (69 pm).[19] We evaluated the lattice parameters evolution with Ga concentration as shown in Fig. 1(c).

Figure 2 shows the surface evolution with doping, as measured by scanning electron microscopy (SEM) and energy dispersive x-ray spectroscopy (EDX) mapping (inset). Figure 2(a) shows a flat surface of undoped Mg_2Sn. As Ga was incorporated, the formation of Ga droplets was observed, as shown in Figs. 2(b) and 2(c). It is likely that the increase in the rate of Ga promotes the formation of droplets that precipitate on the surface. Droplet formation has already been

© Author(s) 2021

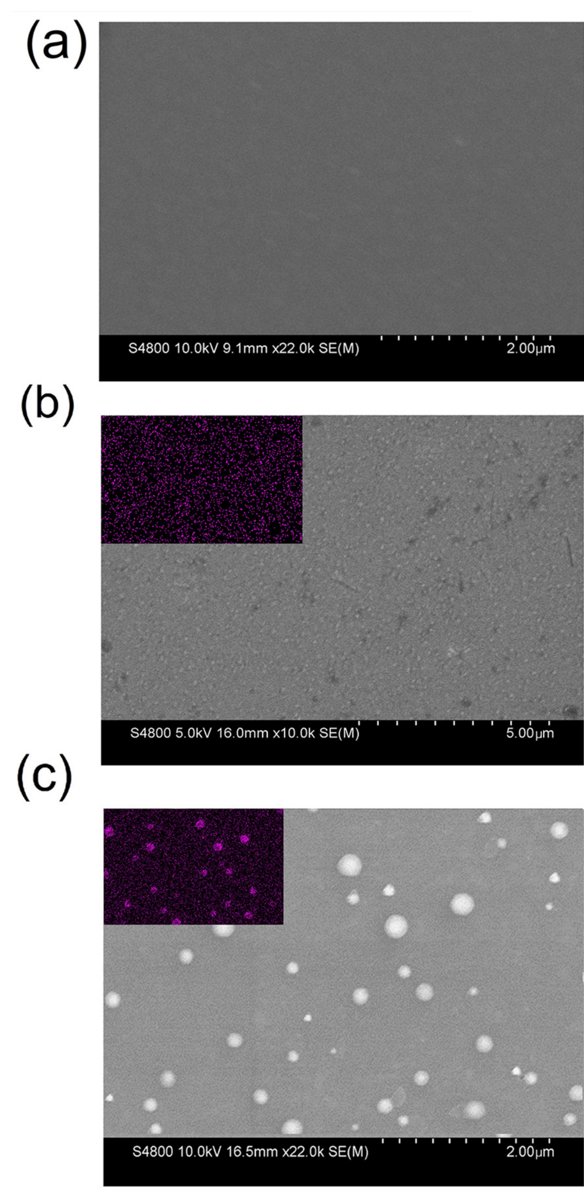

FIG. 2. SEM images and EDX mapping for Ga K_α (inset): (a) Mg_2Sn, (b) $Mg_2Sn_{0.95}Ga_{0.05}$, and (c) $Mg_2Sn_{0.93}Ga_{0.07}$.

reported in the studied for quantum structures in GaAs and Si.[28,29] As the Ga rate increased, the droplets increased. From rough estimation of the droplets diameter (50–200 nm) and their density for the 7 at. % doped sample [Fig. 2(c)], the total amount in the droplets is calculated at less than 0.4 at. %.

Irrespective of Ga contents, thermoelectric properties of $Mg_2Sn_{1-x}Ga_x$ thin films are not greatly influenced by Ga droplets because the total amount volume of Ga droplets is sufficiently small, and most Ga atoms are located inside of thin films. However, the Ga droplet could induce the formation of a non-epitaxial Mg_2Sn orientation as was observed in RHEED in Fig. S2 and in log scale of XRD for highly doped samples in Fig. S3 in the supplementary material.

Thus far, we have explored the effect of Ga incorporation on the microstructure of our thin films. We found that Ga incorporation degrades the epitaxy for our film by the formation of Ga droplets. The reduction in epitaxy and formation of Ga droplets suggest a reduction in the mobility and an increase in carrier concentration. Figure 3 shows the dependence of x on the mobility (μ) and carrier concentration (p) measured at 300 and 180 K. The mobility reaches a peak at around x = 0.03 and shows a reduction, as shown in Fig. 3(a). The first increase can be understood as a change from the intrinsic regime to the extrinsic regime with Ga incorporation. Mg_2Sn has a narrow bandgap approximately 0.3 eV.[9] Therefore, the transition between the intrinsic and extrinsic regimes typically occurs at around 200 K.[30] At room temperature, we are in the intrinsic regime, that is dominated by the lattice scattering that reduces the mobility with temperature ($\mu \sim T^{-3/2}$). However, the incorporation of Ga moves in the extrinsic

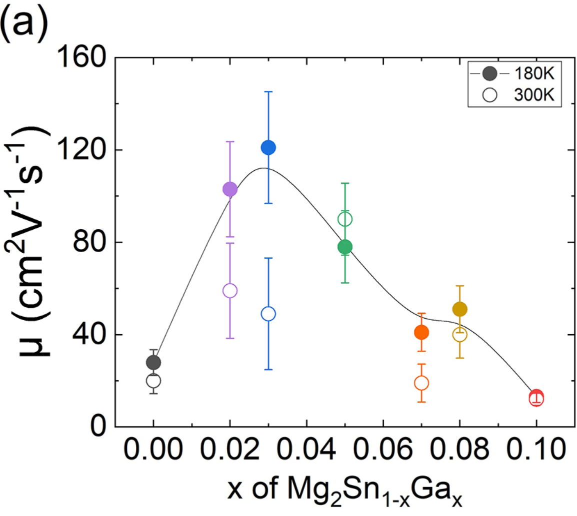

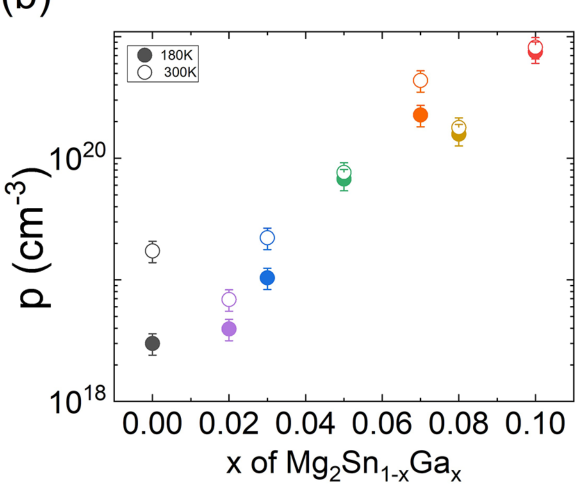

FIG. 3. (a) Mobility and (b) carrier concentration as a function of Ga incorporation.

© Author(s) 2021

regime, and the scattering channel is dominated by the dopant, which increases the mobility in temperature ($\mu \sim T^{3/2}$). The reduction after x = 0.03 can be understood by the degradation of crystallinity due to the formation of Ga droplets, which probably act as scattering centers. The change from intrinsic to extrinsic regime can also be observed in the carrier concentration evolution, as shown in Fig. 3(b). The positive signal and the systematic increase with x suggest that Ga atoms act as hole dopants. The replacement of Ga in the Sn site acts as an acceptor in group 13, decreasing the number of electrons per substitution. In fact, Tani and Kido showed the preference of Ga for Sn sites in the case of the Mg-rich regime by first principles calculations.[18]

The thermoelectric properties of $Mg_2Sn_{1-x}Ga_x$ films are depicted in Fig. 4. Figure 4(a) exhibits the dependence σ on temperature. The electrical conductivity systematically increased with the increase in Ga content. The σ values increase from 0.4×10^2 to 15×10^2 S·cm^{-1} at room temperature, as shown inset of Fig. 4(a). These values are comparable with those reported for the bulk single crystal,[11,16,31] suggesting high quality of our thin films. In the literature, Mg-based II–IV semiconductor thin films have been reported to have lower values than the bulk material.[16] The temperature dependence shows three different regimes: (i) For $x < 0.02$, semiconductor behavior was observed. (ii) In the range of $0.02 < x < 0.05$, a transition was observed from metallic at room temperature to semiconductor-like at high temperature. (iii) For $x > 0.05$, it exhibited metallic behavior in the full temperature range measured.

The similar three regimes were also found for the Seebeck coefficient (α), as shown in Fig. 4(b). The undoped sample has a transition from p- to n-type at 400 K and a strong dependence with temperature, which is due to the small difference between the major and minor carrier numbers, that is, the bipolar effect. The same behavior has been reported for single- crystal bulk materials.[11,30] Similarly, x = 0.02 shows a strong dependence on temperature dependence. In $0.02 < x < 0.05$, strong p-type behavior was observed without temperature dependence. For $x > 0.05$, a weak p-type Seebeck coefficient was observed, with a slight temperature dependence.

The Ga incorporation systematically shifts from intrinsic to extrinsic regime behavior by increasing the carrier concentration. In conductivity, the improvement is a combination of high mobility and an increase in the carrier concentration. From the XRD data, the change in the lattice parameters was not strong, suggesting that the Ga incorporation is insufficient for deformation of the electronic band structure, but it is enough to form doping states. As the carrier concentration increases, the doping states probably increase too and act as scattering center close to a valence band. For undoped and $x < 0.03$, the density of doping states is small, a small amount of energy could ionize the impurities states and thermally excite holes and electrons across the bandgap by the bipolar effect. However, for $x > 0.03$, the number of impurity states is large; consequently, the impurity states become dominant before activation the bipolar effect. Probably, this bipolar onset shift to higher temperature causes the temperature shift for the maximum Seebeck coefficient.

A similar behavior was reported by Chen and Savvides in Ag-doped polycrystalline Mg_2Sn.[31,32] Shi and Kioupakis predicted the Seebeck coefficient behaviors of Mg_2Si, Mg_2Ge, and Mg_2Sn as a function of carrier concentration and temperature by a theoretical study based on the GW-method that includes with spin–orbit coupling.[33] Comparing our experimental data with their calculation, our results were in a good agreement with the calculation, as shown in Fig. S4 in the supplementary material. This suggests that the incorporation of Ga changes the hole carrier concentration and induces the shift of a Fermi level and the formation of a dopant level. The doping level will compete with the bipolar effect and increase the bipolar temperature onset to a higher temperature.

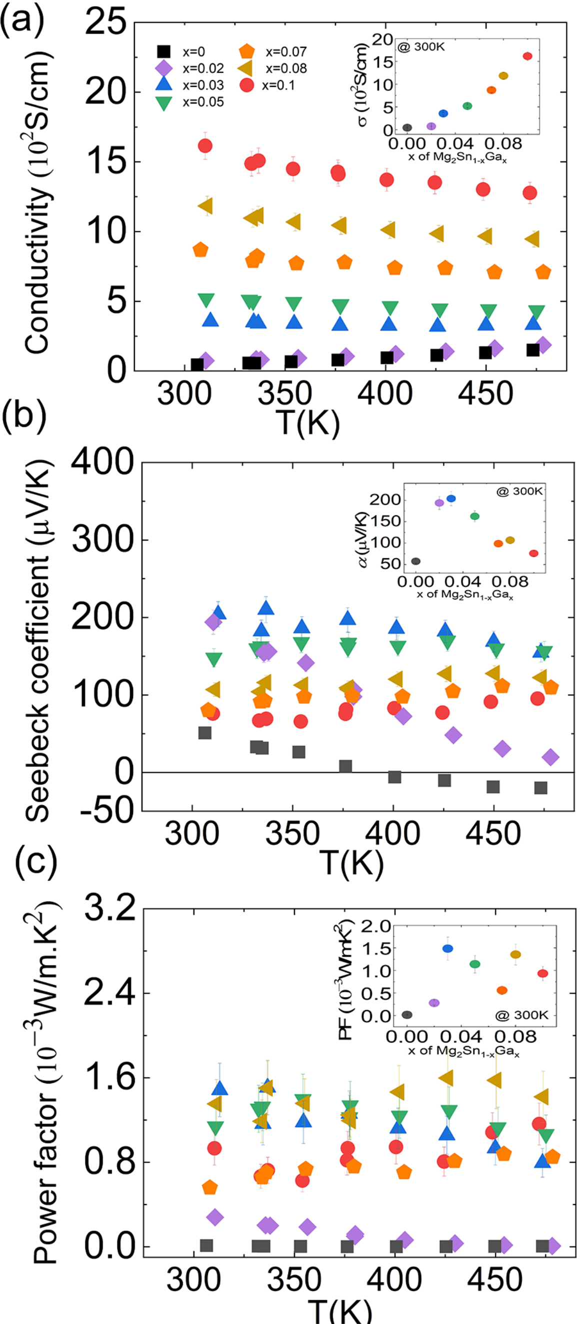

FIG. 4. (a) Electrical conductivity, (b) Seebeck coefficient, and (c) power factor as the function of the temperature of $Mg_2Sn_{1-x}Ga_x$ (x = 0, 0.02, 0.03, 0.05, 0.07, 0.08, and 0.1).

© Author(s) 2021

Figure 4(c) shows the temperature dependences of PF ($\alpha^2\sigma$) of the $Mg_2Sn_{1-x}Ga_x$ films. The undoped and lightly doped samples showed a reduction as temperature increase in PF. For $0.03 < x < 0.05$, the PF is almost constant at 1.0×10^{-3} W·m^{-1}·K^{-2} in all temperature ranges. For highly doped samples, an increase with temperature was observed. The PF value was improved by approximately 100 times with the incorporation of Ga. The maximum value reaches 1.49×10^{-3} W·m^{-1}·K^{-2} at 300 K for $Mg_2Sn_{0.97}Ga_{0.03}$, as shown in inset of Fig. 4(c). This value is comparable to that of the best p-type Mg-based bulk II–IV semiconductors at room temperature. This is the highest value reported in the case of Mg_2Sn thin films.

Figure 5(a) shows the thermal conductivities of the $Mg_2Sn_{1-x}Ga_x$ films, which were measured by a modified picosecond thermoreflectance apparatus.[34,35] The thermal conductivity values are comparable with those reported for bulk Mg_2Sn.[11,16,30,36] The high values can be attributed to the epitaxial nature of the thin films, which act as single crystals. The thermal conductivity behaviors can be divided into two regimes: For $x < 0.05$ of $Mg_2Sn_{1-x}Ga_x$ solid solutions, thermal conductivity slightly decreases with an increase in Ga concentration, suggesting that Ga acts as an effective phonon scatter. For $x > 0.05$, of a mixed phase, composed of Ga dropets and Ga-doped Mg_2Sn, the thermal conductivity is a mixture of contributions that is difficult to distinguish.

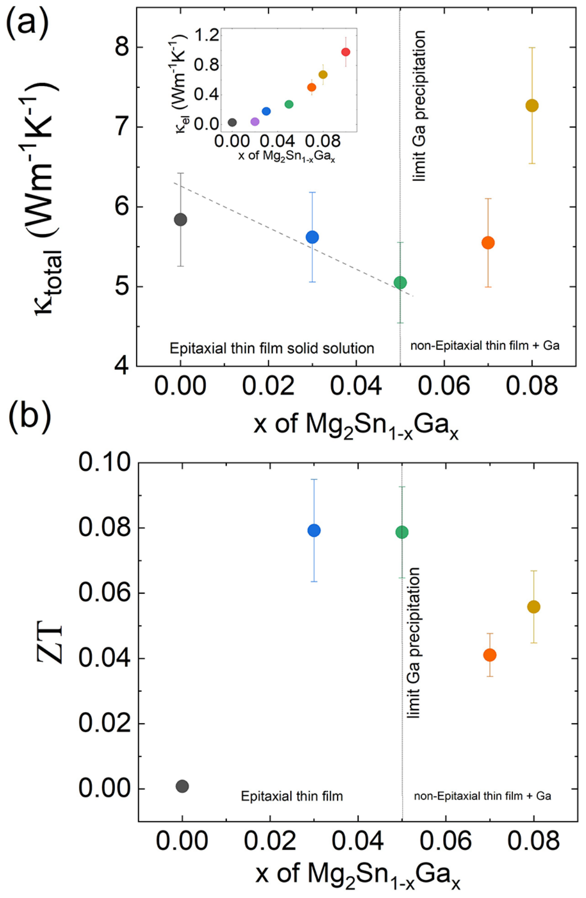

FIG. 5. (a) Total thermal conductivity at room temperature, (b) ZT as the function of Ga incorporation.

The total thermal conductivity (κ) is sum of electronic (κ_{el}), bipolar (κ_{bip}), and lattice (κ_{latt}) contributions. The electronic contribution is $L\sigma T$, where L is the Lorenz number and σ is the measured electrical conductivity as shown in Fig. 4(a). The Lorenz number can be estimated from the Seebeck coefficient ($L = 1.5 + \exp[-|S|/116]$, S in μV·K^{-1} and L in 10^{-8} Ω·W·K^{-2}).[37] The accuracy of the estimation will depend on the band structure of the material and scattering mechanism. Kim *et al.* suggested that the deviation is approximately 20% for non-single band regimes.[37] The inset of Fig. 5(a) shows the evolution of κ_{el} with x. Although the electronic contribution increases with Ga incorporation, the total thermal conductivity decreases, indicating that the bipolar and lattice contributions are dominant.

The bipolar contribution is given by the Peltier heat flows that occur by the recombination of two types of carriers: $\kappa_{bip} = [\sigma_n \sigma_p/(\sigma_n + \sigma_p)] (\alpha_p - \alpha_n)^2 T$, where σ_n, σ_p, α_p, and α_n are the electron and hole electrical conductivities and Seebeck coefficient.[38] In Mg_2Sn, the bandgap reduces with the temperature ($E_g = 0.30 + \beta T$, $\beta = -3.2 \times 10^{-4}$ eV/K),[39] which affect the thermal excitation carrier and the temperature onset of bipolar transport. In bulk material, the bipolar effect is avoided by atomic substitution, which increases the bandgap.[40] The behaviors of Seebeck coefficient indicate the strong bipolar effect in undoped and lightly doped samples, but weak in heavily doped ones, suggesting that the bipolar contribution could decrease with an increase in doping concentration.

The lattice contribution can be described by three scattering processes: dislocation (τ_d), Umklapp processes (τ_U), and point defects (τ_{pd}). From Matthiessen's rules, the inverse of the total relaxation time can be expressed as the sum of the inverse individual contributions ($\tau_{total}^{-1} = \tau_d^{-1} + \tau_U^{-1} + \tau_{pd}^{-1}$). From the Debye model, the total relaxation time is proportional to the lattice contribution.[41] Between the three scattering processes, the point defect scattering has a clear relationship with the Ga incorporation. According to the Callaway–Klemens model,[41] which was recently reviewed by Gurunathan *et al.*,[42] the mass difference, chemical bonding, and atomic radius are proportional to the point defect scattering parameter (Γ), which reduces the point defect relaxation time. Consequently, the lattice combination decreases. Our results of XRD data and Hall effect measurements imply that Ga atoms locate at Sn site. Therefore, Ga will act as a phonon-defect scattering center and reduces the lattice thermal conductivity because of the differences of the atomic mass, chemical bonding, and the modulation effects of chemical bonding induced by the partial substitution of Ga for Sn site. In addition, a possible vacancy in the Mg site (V_{Mg}) may act as a scattering center. In fact, the reduction in thermal conductivity induced by point defects in single crystals of Mg_2Sn was reported by Saito *et al.*[16] For a deeper understanding, further investigations are required.

The values of ZT at room temperature in $Mg_2Sn_{1-x}Ga_x$ thin films are exhibited in Fig. 5(b). The maximum ZT value of 0.08 at room temperature was obtained for $Mg_2Sn_{0.97}Ga_{0.03}$. The result is of the same order as that in the bulk materials: 0.06 for Na doped-Mg_2Sn,[43] 0.08 for Li doped-Mg_2Sn,[43] and 0.14 for Ag–Mg_2Sn,[30,32] suggesting that doped epitaxial thin films in Mg-based materials could be a promising way to achieve high efficiency in small thermoelectric devices.

In conclusion, we fabricated $Mg_2Sn_{1-x}Ga_x$ epitaxial thin films on sapphire (0001) substrates by MBE and investigated the influence of

© Author(s) 2021

Ga doping on the structural and thermoelectric properties of the films. An epitaxially grown thin film is vital to achieve high carrier mobility, which improves conductivity. The positive carrier concentration increased with x, suggesting that Ga atoms act as acceptors effectively doping the Sn sites of the films. Seebeck coefficient behaviors in our experimental study are in good agreement with theoretical calculations in the literature. The onset temperature of bipolar behavior was shifted to higher temperatures in the Seebeck coefficient and electrical conductivity. The combination of both effects resulted in improved PF values, which were close to those of the best bulk materials. The optimal PF value was $\alpha^2\sigma = 1.49 \times 10^{-3}$ W·m^{-1}·K^{-2} at 300 K for $Mg_2Sn_{0.97}Ga_{0.03}$. In the thermal conductivity, Ga doping reduced the lattice contribution likely from the mass contrast effect. The thermal conductivity values were higher than those expected for a thin film; however, they could be further improved by atomic substitution or point defect engineering.

See the supplementary material for the experimental section methods; RHEED pattern, log scale XRD, and comparison of theoretical curves from the literature and our experimental data from Seebeck coefficient (Fig. S4).

M.S.L.L. acknowledges the Japanese Government for providing financial assistance to conduct this work through the Monbukagakusho (MEXT) scholarship. Support from Nos. JST JPMJMI19A1 and JSPS JP16H06441 is acknowledged.

AUTHOR DECLARATIONS

Conflict of Interest

The authors declare no conflict of interest.

DATA AVAILABILITY

The data that support the findings of this study are available from the corresponding authors upon reasonable request.

REFERENCES

[1] T. Mori and S. Priya, MRS Bull. **43**, 176 (2018).
[2] I. Petsagkourakis, K. Tybrandt, X. Crispin, I. Ohkubo, N. Satoh, and T. Mori, Sci. Technol. Adv. Mater. **19**, 836 (2018).
[3] L. E. Bell, Science **321**, 1457 (2008).
[4] B. C. Sales, Science **295**, 1248 (2002).
[5] H. E. Jian and T. M. Tritt, Science **357**, 9997 (2017).
[6] T. Mori, Small **13**, 1702013 (2017).
[7] Y. Xiao and L. D. Zhao, Science **367**, 1196–1197 (2020).
[8] Z. Liu, N. Sato, W. Gao *et al.*, Joule **5**, 1196 (2021).
[9] V. K. Zaitsev, *Thermoelectric Handbook Macro to Nano* (CRC Press, 2006).
[10] R. Santos, S. A. Yamini, and S. X. Dou, J. Mater. Chem. A **6**, 3328 (2018).
[11] X. Li, S. Li, S. Feng, and H. Zhong, Intermetallics **81**, 26 (2017).
[12] X. Li, S. Li, S. Feng, and H. Zhong, J. Alloys Compd. **739**, 705 (2018).
[13] W. Saito, K. Hayashi, Z. Huang, J. Dong, J.-F. Li, and Y. Miyazaki, ACS Appl. Mater. Interfaces **12**, 57888 (2020).
[14] K. Hayashi, W. Saito, K. Sugimoto, K. Ohoyama, K. Hayashi, N. Happo, M. Harada, K. Oikawa, Y. Inamura, and Y. Miyazaki, AIP Adv. **10**, 035115 (2020).
[15] W. Saito, K. Hayashi, Z. Huang, K. Sugimoto, K. Ohoyama, N. Happo, M. Harada, K. Oikawa, Y. Inamura, K. Hayashi, T. Miyazaki, and Y. Miyazaki, ACS Appl. Energy Mater. **4**, 5123 (2021).
[16] W. Saito, K. Hayashi, J. Dong, J. Li, and Y. Miyazaki, Sci. Rep. **10**, 2020 (2020).
[17] Z. M. Gibbs, H. S. Kim, H. Wang, and G. J. Snyder, Appl. Phys. Lett. **106**, 022112 (2015).
[18] J. Tani and H. Kido, Physica B **407**, 3493 (2012).
[19] R. D. Shannon, Acta Crystallogr., Sect. A **32**, 751 (1976).
[20] N. Nandihalli, C.-J. Liu, and T. Mori, Nano Energy **78**, 105186 (2020).
[21] S. Lee, S. Kim, A. Pathak, A. Tripathi, T. Qiao, Y. Lee, H. Lee, and H. Y. Woo, Macromol. Res. **28**, 531 (2020).
[22] A. Katagiri, S. Ogawa, T. Shimizu, M. Matsushima, K. Akiyama, H. Uchida, and H. Funakubo, Jpn. J. Appl. Phys., Part 1 **59**, SF1001 (2020).
[23] A. Katagiri, S. Ogawa, M. Uehara, P. S. Sankara Rama Krishnan, M. Kurokawa, M. Matsushima, T. Shimizu, K. Akiyama, and H. Funakubo, J. Mater. Sci. **53**, 5151 (2018).
[24] T. Aizawa, I. Ohkubo, M. S. L. Lima, T. Sakurai, and T. Mori, J. Vac. Sci. Technol. A **37**, 61513 (2019).
[25] M. S. L. Lima, T. Aizawa, I. Ohkubo, T. Sakurai, and T. Mori, Jpn. J. Appl. Phys., Part 1 **60**, SBBF06 (2021).
[26] H. Le-Quoc, S. Béchu, S. Populoh, A. Weidenkaff, and A. Lacoste, J. Alloys Compd. **546**, 138 (2013).
[27] Z. J. Chen, B. Y. Zhou, J. X. Li, and C. L. Wen, Appl. Surf. Sci. **386**, 389 (2016).
[28] H. Detz, M. Kriz, D. MacFarland, S. Lancaster, T. Zederbauer, M. Capriotti, A. M. Andrews, W. Schrenk, and G. Strasser, Nanotechnology **26**, 315601 (2015).
[29] C. Heyn, A. Stemmann, A. Schramm, H. Welsch, W. Hansen, and Á. Nemcsics, Phys. Rev. B **76**, 075317 (2007).
[30] H. Y. Chen, N. Savvides, T. Dasgupta, C. Stiewe, and E. Mueller, Phys. Status Solidi A **207**, 2523 (2010).
[31] H. Y. Chen and N. Savvides, J. Electron. Mater. **39**, 1792 (2010).
[32] H. Y. Chen and N. Savvides, J. Cryst. Growth **312**, 2328 (2010).
[33] G. Shi and E. Kioupakis, J. Appl. Phys. **123**, 85114 (2018).
[34] W. Gao, Z. Liu, T. Baba, Q. Guo, D. Tang, N. Kawamoto, E. Bauer, N. Tsujii, and T. Mori, Acta Mater. **200**, 848 (2020).
[35] Y. Kakefuda, K. Yubuta, T. Shishido, A. Yoshikawa, S. Okada, H. Ogino, N. Kawamoto, T. Baba, and T. Mori, APL Mater. **5**, 126103 (2017).
[36] N. Savvides and H. Y. Chen, J. Electron. Mater. **39**, 2136 (2010).
[37] H. S. Kim, Z. M. Gibbs, Y. Tang, H. Wang, and G. J. Snyder, APL Mater. **3**, 041506 (2015).
[38] T. M. Tritt, *Thermal Conductivity: Theory, Properties and Applications* (Kluwer Academic/Plenum Publisher, New York, 2004), p. 112.
[39] H. G. Lipson and A. Kahan, Phys. Rev. **133**, A800 (1964).
[40] L. Zhang, P. Xiao, L. Shi, G. Henkelman, and J. B. Goodenough, J. Appl. Phys. **117**, 155103 (2015).
[41] J. Callaway and H. C. Von Baeyer, Phys. Rev. **120**, 1149 (1960).
[42] R. Gurunathan, R. Hanus, M. Dylla, A. Katre, and G. J. Snyder, Phys. Rev. Appl. **13**, 034011 (2020).
[43] J. Tani, T. Shinagawa, and M. Chigane, J. Electron. Mater. **48**, 3330 (2019).

© Author(s) 2021